Enhancing electrochemical production of peroxophosphates using new boron doped diamond coatings

L.G. Vernasqui[1]; N. G. Ferreira [1]; C. Saez[2]; M. A. Rodrigo [2]

[1] *Laboratório Associado de Sensores e Materiais, Instituto Nacional de Pesquisas Espaciais (INPE), Av. dos Astronautas, 1758, 12227 010 São José dos Campos, SP, Brazil*

[2] *Electrochemical & Environmental Engineering Lab, TEQUIMA Research Group - Edificio Enrique Costa Novella, Campus Universitario s/n, 13071 Ciudad Real, Spain*

Abstract.

Two boron doped ultrananocristallyne diamond (UNC) electrodes were manufactured and compared with a standard microcrystalline commercial electrode, to clarify how their differences may affect to the production of oxidants in the electrolysis of solutions containing phosphoric acid or phosphate salts. Effects of the current density and electrolyte pH were evaluated. Significant differences were found in the production of oxidants, being the production of oxidants favored, at high current densities and alkaline pHs. The effect of the pH was explained in terms of the higher stability of the peroxodiphosphate anion in comparison with the monoperoxyphosphate acid produced at low pHs. As well, because of the improved electrostatic attraction of the anion with the anode. Despite not exhibiting the largest electrochemical surface area, the flat UNC electrode shows the best performance for this process, except for the operation at low current densities and alkaline pHs in which the porous UNC outperforms it. Better efficiencies are obtained operating at mild current densities which was explained in terms

of the great significance of direct processes in the production of oxidants by electrolysis of phosphoric acid or phosphate solutions

Keywords

Peroxophosphate; monoperoxophosphoric acid; diamond electrodes; electrolysis; ultrananocrystalline, microcrystalline

Graphical Abstract

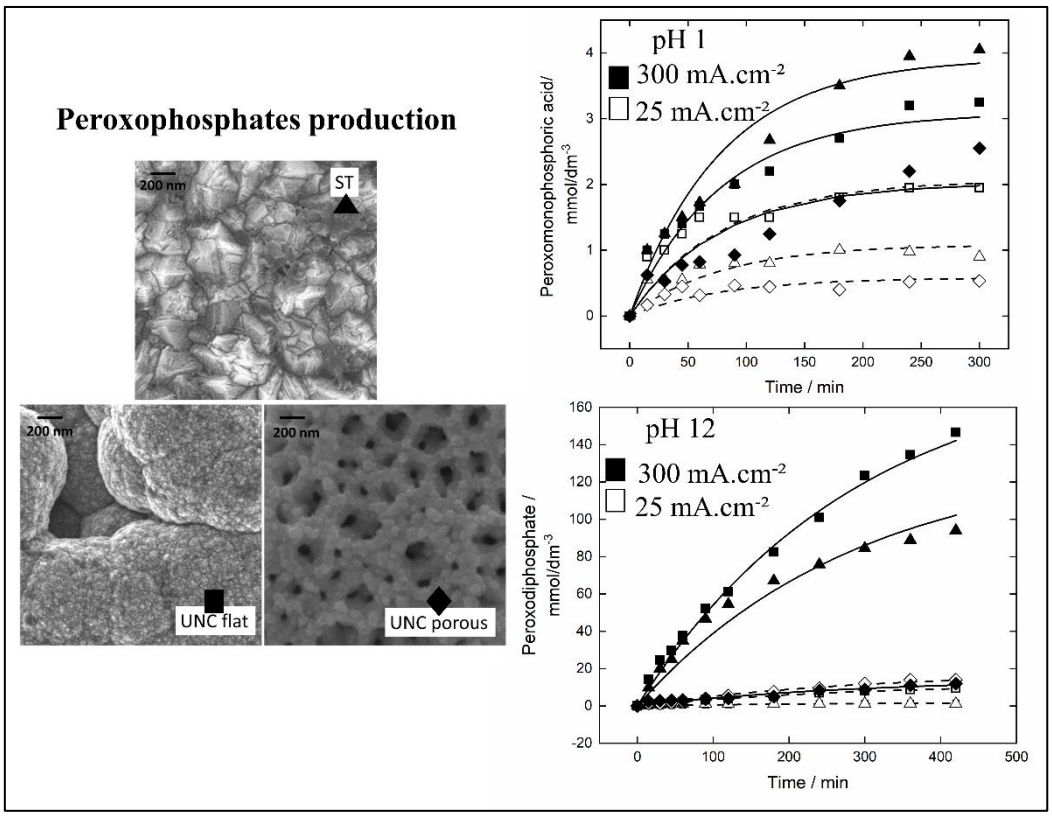

Highlights

- Higher oxidant production at high current densities and with alkaline electrolytes
- Low efficiency of the electrolysis carried out at acidic pHs
- Oxidants production efficiency is highly influenced by diamond coating
- Flat UNC outperforms porous UNC and standard microcrystalline electrodes

Introduction

Production of oxidants using electrochemical technology is known for centuries but, due to the progress made on electrode materials in the last decades, these processes become more attractive than ever [1–4]. One family of compounds with a special interest is the peroxocompounds, which can be considered as acids derivatives in which the group -OH is substituted by a -O-OH [2,5]. This group includes peroxosulphates, peroxocarbonates, peroxonitrates, and peroxophosphates. This work focuses on the last product of the group, which, in fact, is not a single chemical but two different species: the less stable peroxomonophosphoric acid (H_3PO_5), formed at acidic conditions, and the more stable salts of the peroxodiphosphate anion ($P_2O_8^{4-}$), formed at alkaline conditions. In addition to both species, a third commercial product is typically found in the market under the peroxophosphate or perphosphate "label", but it is not real peroxophosphate (because it lacks the peroxo group linked to a phosphorus atom), merely a mixed formulation containing hydrogen peroxide occluded in crystallized phosphate salts (peroxo group is not bonded to the phosphorus atoms).

Although it was reported the electrochemical production of oxidants during the electrolysis of phosphate with platinum anodes for more than seventy years [1,6,7], that process lacked efficiency and the electrochemical production of peroxocompounds obtained by oxidation of phosphate solutions was found to be efficient using diamond coatings [2,8,9], process which was first proposed at the turn of this century, both in alkaline [10] (peroxodiphosphate) and acidic media [11] (monoperoxophosphoric acid).

Peroxophosphates are strong oxidants from the thermodynamic perspective, but the oxidation is kinetically controlled and then, they can be considered as not very hard oxidants unless activated with UV light or other oxidants, as it also happens with other peroxocompounds. The easiness in the recovery of phosphate by precipitation

/redissolution makes them very attractive as an alternative to peroxosulphates in advanced oxidation processes (AOPs) [5,12]. Formation of the radical sulphate by activation of peroxosulphates with other oxidant, UV light or other method is proposed as a very convenient alternative to hydroxyl radicals in recent research works [13–18]. In this context, the chemistry of peroxosulphates and peroxophosphate anions (and acids, as well) is very alike and hence, phosphate radicals may substitute easily sulfate radicals in those applications, with the additional advantage that sulphate anions are more difficult to be separated from water than phosphate ions (which merely need a sequential change in the pH). This means that in developing an effective process for the production of peroxophosphates, and confirming its outstanding properties for the oxidation of organics (which were investigated and pointed out in previous works [19,20]), phosphate radicals can become a real alternative to sulphate radicals in AOP applications [21]. Recently a review [1] indicated the standard reduction potentials of peroxocompounds and showed the similarity between the ionic oxidants $C_2O_6^{2-}$ (1.80 V vs SHE), $S_2O_8^{2-}$ (2.01 V vs SHE) $P_2O_8^{2-}$ (2.07 V vs SHE) and that of the radicals $PO_4^{\bullet 2-}$ (2.26 V vs SHE) and $SO_4^{\bullet -}$ (2.4 V vs SHE).

In previous work, it was found that characteristics of the diamond coating and substrate influenced very importantly on the peroxophosphate production process performance [22]. In fact, it was investigated the effect of the diamond doping level, sp^3/sp^2 ratio, and thickness of the diamond coating and it was found that this later parameter was of outstanding significance, which was explained in terms of the interactions of silicon (substrate onto which the coating was deposited) with phosphates. This effect of the substrate was further investigated in a more recent work during the formation of peroxosulphates in which, again, the positive effect of silicon was pointed out within comparison with the use of substrates of niobium and tantalum substrates [23].

Now, we want to retake the topic with a new approach based on the development of special diamond coatings that do not promote but prevent the massive formation of hydroxyl radicals, favoring direct electrochemical surfaces with a larger surface area, and try to determine how efficient is the manufacturing of this important chemical. This will allow to understand better the oxidation mechanisms that develop on the diamond surface and help to optimize the production of peroxophosphate, with the view of a near increase in the technology readiness level of the generation technology. To do this, two novel anodes with boron doped ultra-nanocrystalline diamond (UNC) coating were manufactured and compared with a commercial standard microcrystalline electrode in terms of peroxophosphate production at two different current densities: one softer (25 mA cm^{-2}) and one harsher (300 mA cm^{-2}) to clarify how electrodic surface area may influence on the production of oxidants with acidic and alkaline phosphoric acid/phosphate aqueous electrolytes. Results obtained allow to understand much better the complex formation of these powerful oxidants and give important conclusions for future works.

2 Materials & Methods

Diamond coatings. Three different electrodes were used for peroxophosphates production. Two of them present ultrananocrystalline morphology and were produced by our research group using hot filament chemical vapor deposition (HF – CVD). In this technique, a vacuum pump induces a vacuum in the system and the gas mixture is introduced into the reactor with proportions adjusted by flow controllers. After adjustment for the growth pressure, the energy source (DC SUPLITEC, model FA 5040 with a capacity of 50 V and 40 A) which is connected to the copper electrodes that support the filaments controls the current to maintain the suitable temperature for the coating growth. The substrate temperature was determined by a K-type thermocouple. After

reaching the growth temperature, an additional line of H_2 is opened and the flux is responsible for dragging the boron that evaporates by the action of the thermostatic bath which contains the bubbler containing boron diluted in methanol. Both coatings were obtained after 7 h of growth and the temperature and pressure were maintained at 650 ºC and 30 Torr, respectively. The B/C ratio for the dopping was 30,000 ppm and the growth atmosphere was 85% argon, 13% hydrogen, and 2% methane.

The first coating (named UNC flat) is coated above a Ti sheet using a seeding conventional pre-treatment procedure to obtain boron-doped electrodes [24], and the second (named UNC porous) presents porosity and is coated above titanium dioxide nanotubes without the seeding pre-treatment [25]. The third electrode is a commercial boron-doped diamond electrode with microcrystalline morphology purchased from Adamant (named ST). It is important to mention that all the electrodes presented the same geometric area: 2 cm^2.

Electrodes characterization. Scanning electron microscopy was used to evaluate the morphology of the three electrodes (FEG-SEM; Zeiss Gemini SEM 50). Electrochemical measurements were performed using a conventional three-electrode cell connected to a computer-controlled Autolab potentiostat/galvanostat model PGSTAT 302N. The three diamond electrodes were used as work electrodes and an Ag/AgCl (3M KCl) and platinum were used as reference and counter electrodes, respectively. Cyclic voltammograms (CV) in the presence of 1 mM of $[Fe(CN)_6]^{3-/4-}$ (1M Na_2SO_4) were recorded in different scan rates (5 – 500 $mV.s^{-1}$) and the Sevcik equation was used to estimate the electrochemical area of the electrodes [26,27]. In addition, linear voltammograms were obtained using the bulk electrolyte with pH 1 and 12, and the Tafel plot was also evaluated.

Analytical procedures. The peroxophosphates electrogenerated were measured using iodometric titration [28]. In this methodology, potentiometric titrations with thiosulphate in an acid medium were conducted and the oxidant species capable of oxidizing I^- to I_3^- are quantified.

Oxidant production process. Electrochemical oxidant production was carried out using a setup with the same elements described in previous works about the production of peroxophosphates [5] and equipped with a 3-D printed flow cell consisting of two polymer plates (10.0 cm x 6.5 cm), mechanized each of them with one electrode housing (2.5 cm x 2.5 cm) in the central part in which the electrodes to be tested were placed. In this system, the electrolyte (1M H_3PO_4 – pH 1 or 12) contained in a reservoir passes through a pump with flow control, responsible for inducing the flow (50 $L.h^{-1}$) to the electrochemical cell that supports the cathode (steel) and anode (diamond films). The electrodes are connected to an energy source that applies the potential difference between the electrodes necessary for electrolysis (25 and 100 $mA.cm^{-2}$). Also, the system is equipped with a heat exchanger connected to a thermostatic bath to control the temperature of the system at 25ºC. The solution pH was maintained at alkaline value by adding potassium hydroxide and the pH was monitored using a WTW-InoLab pH meter and the aliquots to iodometric measurement were collected from the reservoir, using a pipette.

The reproducibility of the different electrodes was evaluated by a reproducibility test that was performed by a three-time repetition electrolysis analysis. The results suggested that the error of the electrodes in oxidant production is ±0.26, ±0.32 and, ±0.4 $mmol.dm^{-3}$ for UNC, UNC porous and, Standard electrodes, respectively.

3 Results and Discussion

Electrodes characterization. Figure 1 shows SEMs images of the electrodes evaluated in this work. As seen, the two electrodes manufactured in our lab presented an ultrananocrystalline morphology, characterized by an average crystallite size above 10 nm and the common "ballas" diamond structure [29,30]. In Fig 1 C, it can be observed that the surface of the porous UNC is formed by inner (~60nm) and outer pores (200-250 nm). Additional details about its morphology and structure are described elsewhere [25]. In comparison, the ST electrode presented an average crystallite size of 0.2 – 0.4 µm and the characteristic morphology of microcrystalline films [31,32].

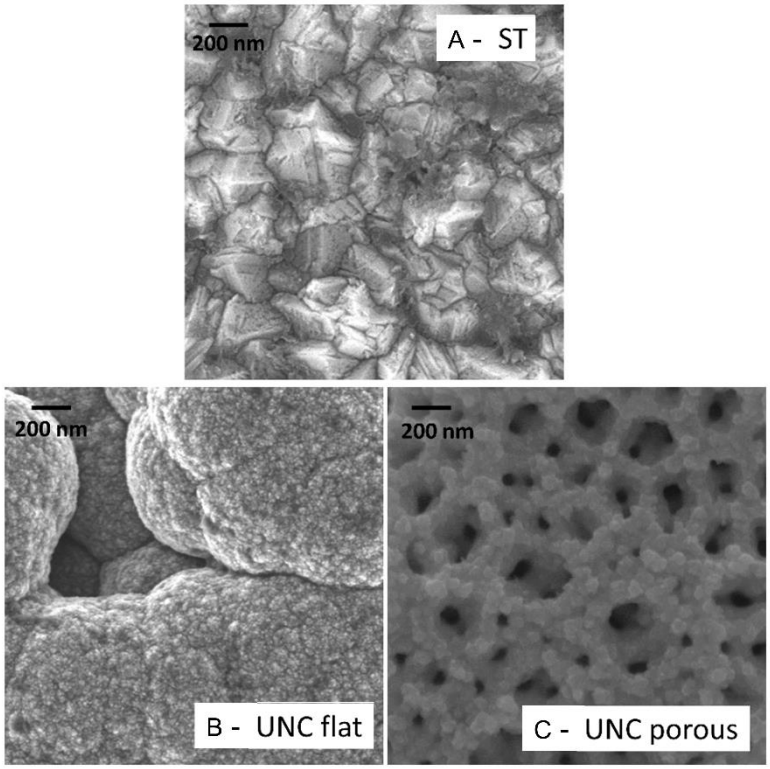

Fig. 1 – SEM images of the electrodes A) Standard, B) UNC flat and, C) UNC porous.

As a result of the smaller size of the crystals as well as the higher renucleation promoted by the Argon on the sample's growing atmosphere [33,34], the surface areas of the two UNC coatings are much higher, and so it is expected to be the electrochemical response

of these electrodes. In addition, the two UNC differs importantly because one of them (UNC porous) showed a more porous frame which also is expected to influence the surface area. This is confirmed by the voltammetric measurements, made with the couple $Fe(CN)_6^{3-}/Fe(CN)_6^{4-}$ and shown in Figure 2, in which it can be seen the larger electrochemical response of the UNC electrodes (higher current densities for the same potential applied), and the more reversible behavior of the pair $Fe(CN)_6^{3-}/Fe(CN)_6^{4-}$ that indicate a higher contribution of the surface processes, that is, of the direct exchange of electrons with the UNC coating [27,35]. This is especially important in the porous UNC. The three electrodes present good reversibility at slow scan rates, with similar values ratio between anodic and cathodic peaks (around 1.3 for Ipa/Ipc ratio), showing that the processes are quasi-reversible and controlled by diffusion [27]. However, the commercial electrode presented a wider ΔEp (between the anodic and cathodic peaks) showing slower electron transfer.

From these figures, it can be obtained the electrochemical surface area with the Sevcik equation [26,27]. As seen in Part D, the area of the flat UNC is more than double of that of the commercial, while the porous UND triplicates this value.

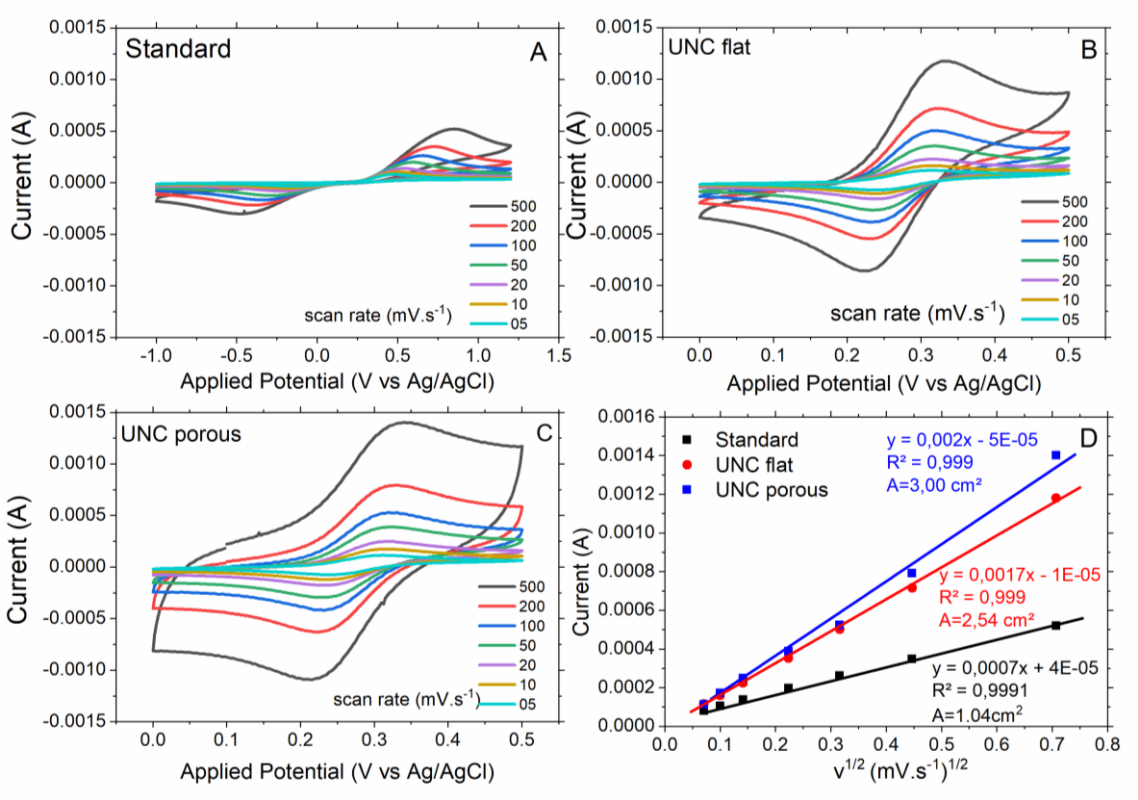

Figure 2. CV measurements performed at different scan rates in $Fe(CN)_6^{3-}/Fe(CN)_6^{4-}$ redox par for the electrodes A) standard; B)UNC flat and, C) UNC porous; and D) the square root of the scan rate versus anodic peak intensity for the different electrodes.

Bulk peroxodiphosphate anion/ peroxomonophosphoric acid production. The three electrodes, aimed to be evaluated in this work, were tested in a flow cell to produce oxidants from the electrolysis of solutions containing sodium phosphate at pH 12 and phosphoric acid solutions at pH 1, applying both:

- a soft current density of 25 mA cm^{-2}, for which the effect of hydroxyl radicals is not expected to be very important, and direct interaction of phosphate with the electrode is expected to define the primary production mechanism, and,
- a harsh current density of 300 mA cm^{-2}, for which radical-based reactions are expected to control the process.

Results during the electrolysis carried out to the acidic electrolyte are shown in Figure 3, where it can be seen that the produced concentration of oxidants increased to reach a steady state concentration in about 4 hours.

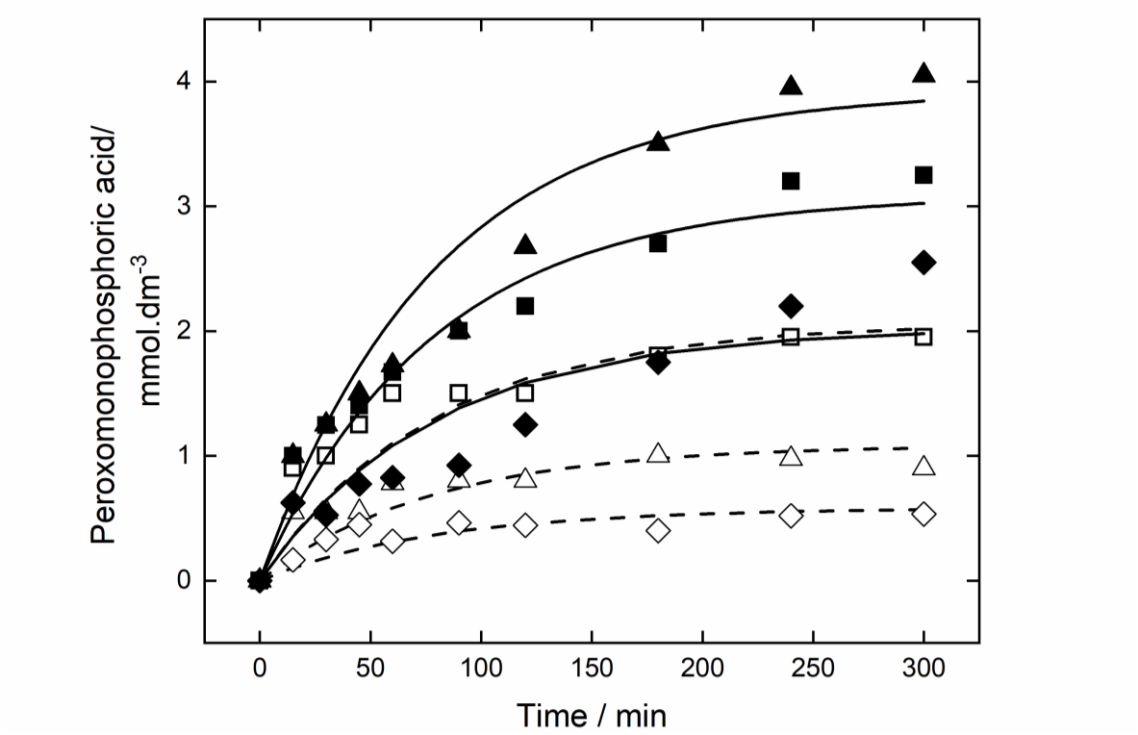

Fig.3– Peroxomonophosphoric acid production ◢ST 300 mA cm^{-2}; ■ flat UNC 300 mA cm^{-2}; ◆ porous UNC 300 mA cm^{-2}; △ ST 25 mA cm^{-2}; □ flat UNC 25 mA cm^{-2} ◇ porous UNC 25 mA cm^{-2}.

It is important to take in mind that although all oxidants measured have been quantified as peroxomonophosphoric acid in the plot, this quantification can only be seen as an approach, because there are no possibilities of measuring accurately the concentration of this particular species in the reaction mixture, where in fact, a cocktail of oxidants is being formed and undergo important interactions even promoted with the changes produced by the analytical techniques used to measure them. Thus, in acidic conditions, peroxomonophosphoric acid is the primary species expected (eq 1), but the occurrence of

ozone [36–39], also generated anodically either from water (eq 2) or from oxygen (eq 3), promoted in acidic conditions, or other oxidants, like the cathodically generated hydrogen peroxide [40–43] (eq. 4), cannot be excluded. Anyway, because of the high concentrations of phosphoric acid, all these species will be produced not as primary but as residual species.

$$H_3PO_4 + H_2O \rightarrow H_3PO_5 + 2H^+ + 2e- \quad (1)$$

$$3H_2O \rightarrow O_3 + 6H^+ + 6e^- \quad (2)$$

$$H_2O + O_2 \rightarrow O_3 + 2H^+ + 2e^- \quad (3)$$

$$O_2 + 2H^+ + 2e^- \rightarrow H_2O_2 \quad (4)$$

Typically, this production of multiple products made chemical characterization very complex, because the different species interact importantly, as shown in eqs 5-7, behaving the less predominant as scavengers of the primary species and contributing not to increase, but to decrease its concentration from the electrolyte. In fact, lifetime of these species is very low and they are very difficult to be detected and only their effect is observed.

$$O_3 + H_3PO_5 \rightarrow 2O_2 + H_3PO_4 \quad (5)$$

$$H_2O_2 + H_3PO_5 \rightarrow O_2 + H_3PO_4 + H_2O \quad (6)$$

$$O_3 + H_2O_2 \rightarrow 2O_2 + H_2O \quad (7)$$

With respect to this scavenging effect, it is important to consider that in bulk production of oxidants in discontinuous operation mode, the steady state reached is explained in terms of the balance between the rates of production and decomposition of the oxidant and it is not always the only response obtained. Thus, during the production of other oxidants like ozone and hydrogen peroxide, instead of a plateau a maximum in the

concentration of oxidant reached is typically observed, which is associated to the production and action of scavengers [44–47].

Regarding the effect of three inputs evaluated (coating, pH, and current density), as seen, operating at high current density allows reaching higher concentrations of the oxidants, although differences are much lower than the changes produced in the current density. Thus, ratios between steady state concentrations reached is 1.5 for flat UNC, 4.8 for porous UNC and 4.0 for ST coatings, while the ratio between the current densities applied is as high as 12. Regarding the effect of the diamond coating, at high current densities the ST electrode outperforms slightly the two UNC electrodes, but this trend reverses at low current densities, where the effect of the direct processes is expected to be more significant. Anyway, differences observed between the three electrodes are not very important, especially if they are compared to those that are going to be obtained during the electrolysis of alkaline solutions.

Thus, Figure 4 shows the results obtained in the electrolysis of alkaline solutions containing sodium phosphate. Again, not a pure oxidant species but a cocktail of oxidants is being formed in the electrolyte during the electrolysis, despite we accounted all oxidants as peroxodiphosphate. In fact, in this case, the primary oxidant expected is the anion peroxodiphosphate (eq 8), which is produced much more efficiently, attaining values as high as 140 mM reached with the UNC electrode after seven hours of electrolysis of the alkaline solution, which is more than 40 times higher than that obtained at acidic conditions at the same current density.

$$2H_3PO_4 \rightarrow H_4P_2O_8 + 2H^+ + 2e^- \qquad (8)$$

This indicates that effects of other oxidants produced electrochemically (ozone, hydrogen peroxide) are completely different from that observed in acidic conditions and their

scavenging action is much lower. Differences between productions obtained at high and low current densities are slightly above 15 $mM.dm^{-3}$ for the flat UNC coating and increase up to 80 $mM.dm^{-3}$ for the ST microcrystalline coating which, opposite to what is observed in the electrolysis of acidic solutions, are much higher than the ratio between the current densities applied (ratio of 12). Surprisingly, this ratio is below 1 in the UNC porous, pointing out that it operates more efficiently under the application of low current densities. In fact, the performance of this electrode is extremely bad at high current densities, what opposed to the performance shown at low current densities where it is the best of the three electrodes evaluated.

As well, it is important to notice that the dynamic response of this electrolysis is slower, and steady-state needs more than 7 hours to be reached, a value that indicates that different processes are happening in comparison with the acidic electrolysis in which in less than 4 hours the system was stabilized. In fact, after seven hours of electrolysis, the concentration of oxidant is not stabilized in any of the tests made.

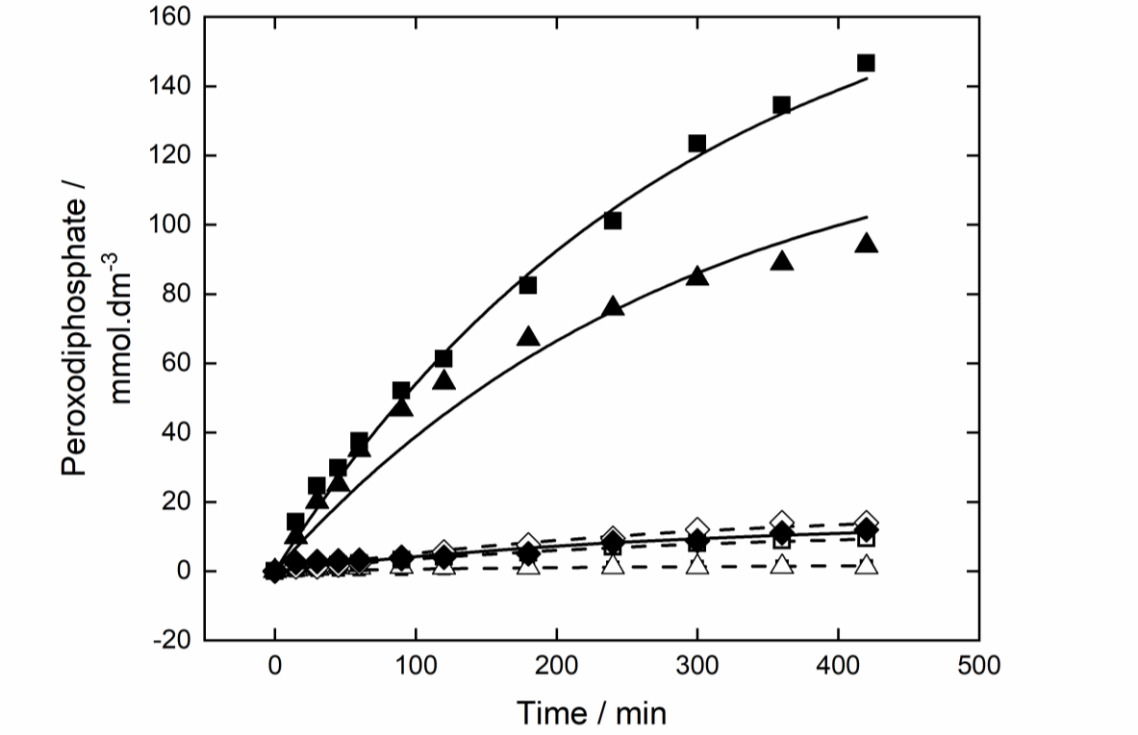

Fig.4– Peroxodiphosphate production ◢ST 300 mA cm^{-2}; ■ flat UNC 300 mA cm^{-2}; ◆ porous UNC 300 mA cm^{-2}; ◿ ST 25 mA cm^{-2}; ◻ flat UNC 25 mA cm^{-2} ◇ porous UNC 25 mA cm^{-2}.

The higher productions obtained at alkaline pHs can be explained in terms of the higher stability of the peroxodiphophate anion, as compared to the monoperoxophosphoric acid, as already reported in previous works [10,11]. As well, it is expected a different type of interaction between the surface of the electrodes and the phosphorus species, considering pKas for phosphoric acid are 2.5, 7.20, and 12.35. Thus, it is assumed a higher electrostatic interaction between the surface of the anode and the phosphate and biphosphate ions present at pH 12 than with the molecular phosphoric acid contained in the solution at pH 1, where no electrostatic forces and no electromigration transport mechanisms can develop.

To go further in the understanding of the process, experimental data were fitted to a single phenomenological model that considers the formation and degradation of the phosphorus species under different conditions. The Petersen matrix of this model is shown in Table 1 and lines plotted in Figure 3 and 4 are simulations made with the model, once the best values for the different parameters were obtained following the application of a mathematical fitting procedure.

Table 1. Petersen matrix for the production of peroxophosphates

Process/Species	S_1	S_2	S_3	Kinetics
Peroxophosphate production	-1	+1		I/nF·h
Water oxidation			+1	I/nF·(1-h)

Peroxophosphate decomposition		-1	+1	K[S2]

S_1: phosphate/biphosphate anion for production of peroxodiphosphate or phosphoric acid for production peroxomonophosphoric acid; S_2: peroxodiphosphate or monoperoxophosphoric acid; S_3: oxygen

As seen, the model fits well to experimental results and regressions coefficients were nearly 0.94 for the electrolysis of acidic electrolyte and 0.98 for the electrolysis of alkaline solutions. The value of the decomposition kinetic constant was kept constant in the fitting of all simulations made, in values of 0.0127 min^{-1} and 0.0034 min^{-1} in acidic and alkaline electrolysis, respectively. These values reproduce satisfactorily electrolysis at high and low current densities with the three electrodes, pointing out that pH is the primary input affecting the stability of the products formed, as it was also found in a previous work in which it was also found that stability of the produced peroxomonophosphoric acid produced electrochemically depended not only on temperature but also very importantly on the pH, being several times lower at pH below 5 [48]. This also indicate that there is no cathodic reduction of the formed peroxophosphate species, because the decomposition does not depend on the current applied.

Regarding efficiencies, the fitting of the parameter of the model to reproduce the experimental data resulted in the values reported in Figure 5. These efficiencies are coulombic efficiencies and inform that in the best conditions more than 80% current efficiency can be obtained, while in the worst less than 6% of the current yields the production of oxidant, being the rest of the electric current wasted in the oxidation of water to oxygen, either directly or throughout decompositions processes. The porous UNC reaches the highest efficiency at low current densities (nearly 90%) and the ratios

between efficiencies obtained with the three electrodes at alkaline pHs seems to be very related at low current densities with the electrochemically active surface area. The bad performance of the porous UNC at high current densities is also observed, being the worsts in acidic and alkaline conditions. This behavior can be explained in terms of the evolution of oxygen because the bubbles produced may block the entry into the pores for the solution. Opposite the flat UNC performs always much better than the ST electrode.

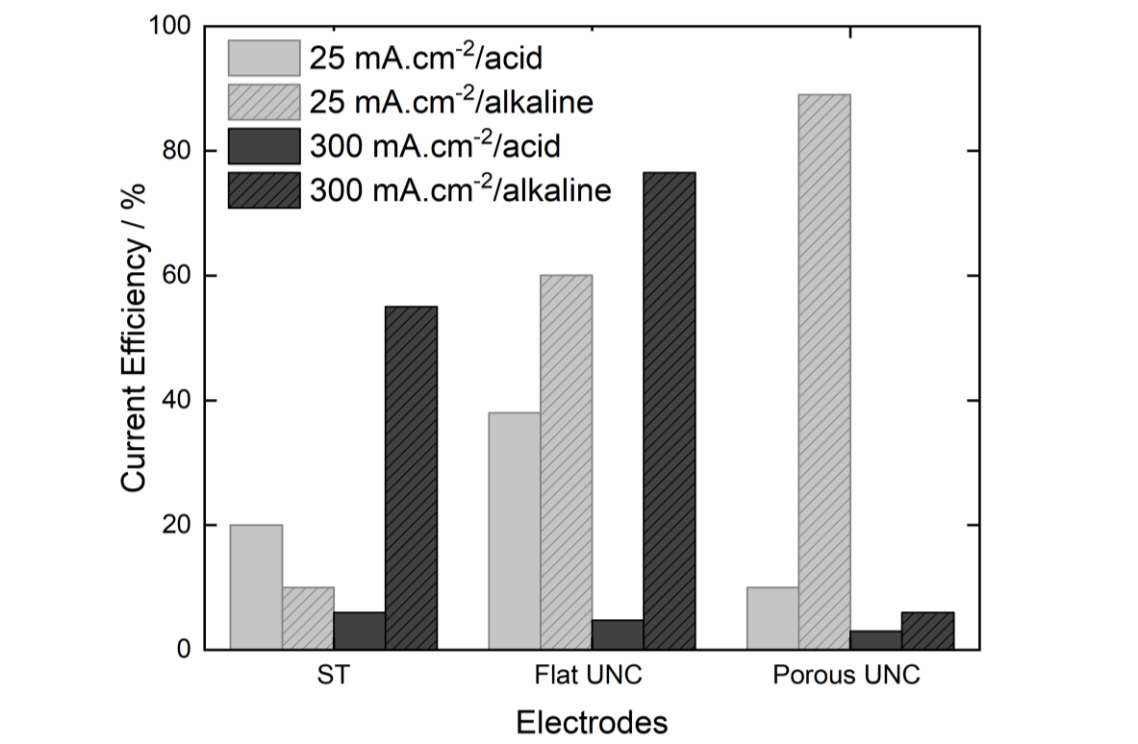

Fig. 5. Efficiencies calculated by mathematical fitting of experimental results.

The behavior observed for the current efficiencies can be better understood with the help of a voltametric evaluation [49], shown in Figure 6, in which it can be seen that the electrochemical window is much smaller operating at alkaline pHs that at acidic pHs.

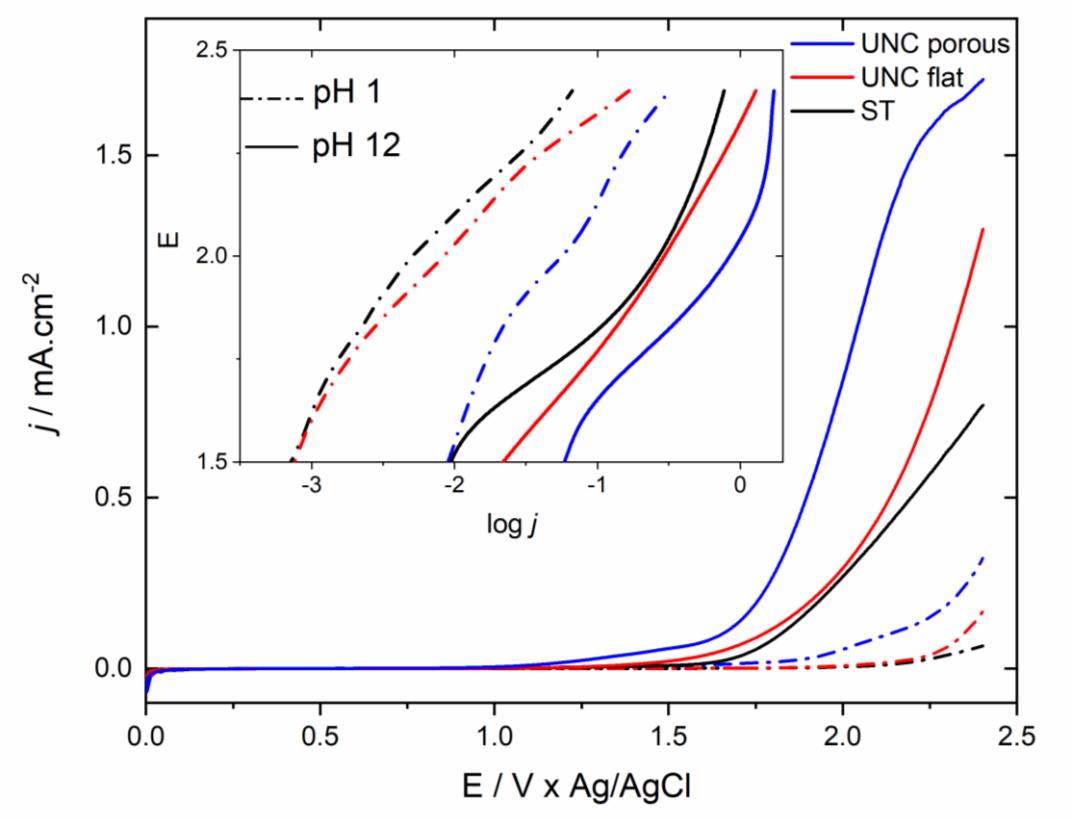

Fig.6 – Polarization curves recorded in 1M phosphoric acid with pH 1 and 12 and Tafel plots (inset).

This observation was explained in previous works in terms of the direct oxidation of the phosphate and biphosphate anions to the corresponding radicals as shown in Eq. 9 [48] and it is supported by considering that current densities exerted for the same potential applied depend on the surface area of the electrode tested, being largest for the porous UNC (with the largest electrode surface area) and lowest for the ST electrodes.

$$PO_4^{3-} \rightarrow (PO_4^{2-})^{\cdot} + e- \qquad (9)$$

This oxidation of phosphate to the radical is not expected to develop at acidic conditions and the much wider electrochemical window indicates that oxidation observed

corresponds to the oxygen evolution with the previous formation of hydroxyl radicals as shown in eq. 10.

$$H_2O \rightarrow (OH)^{\cdot} + H^+ + e^- \qquad (10)$$

The combination of phosphate radicals (eq 11) is a feasible mechanism to explain the very high efficiency observed at alkaline pHs.

$$(PO_4^{2-})^{\cdot} + (PO_4^{2-})^{\cdot} \rightarrow P_2O_8^{4-} \qquad (11)$$

Alternatively, formation of the phosphate and biphosphate radicals can be also mediated by hydroxyl radicals as shown in eq 12.

$$PO_4^{3-} + OH^{\cdot} \rightarrow (PO_4^{2-})^{\cdot} + OH^{\cdot} \qquad (12)$$

However, this process may involve the formation of other oxidants that act as scavengers of peroxodiphoshate (mainly ozone and hydrogen peroxide), and the interactions between these scavengers and phosphate can be promoted by the largest area of the porous UNC, which in turn, can explain the very low efficiency observed in that case.

Regarding acidic conditions, formation of peroxomonophophoric acid requires the formation of the dihydrogen phosphate radical, either by direct oxidation (eq 5) or by mediated oxidation following formation of hydroxyl radicals (eq 6) and the later interaction of hydroxyl and dihydrogen phosphate radicals. Initially the direct process is not promoted as in the alkaline conditions (as explained because of the electrostatic interactions) and this explain the worse efficiencies reached operating at acidic conditions, which are encouraged at high current densities because of the promoted formation of scavengers.

$$H_3PO_4 \rightarrow (H_2PO_4)^{\cdot} + H^+ + e^- \qquad (13)$$

$$H_3PO_4 + OH^{\cdot} \rightarrow (H_2PO_4)^{\cdot} + H_2O \qquad (14)$$

$$(H_2PO_4)^{\cdot} + OH^{\cdot} \rightarrow H_3PO_5 \qquad (15)$$

Hence, the flat UNC seems to outperform the two electrodes because it has a large surface area but do not promote the scavenging effect. Opposite, the porous UNC is a very convenient electrode for the production of peroxodiphosphate anion because it has very large electrochemical surface area and promotes the formation of the oxidant by direct processes in which hydroxyl radicals are not involved when operating at low current densities.

4 Conclusions

From this work, the following conclusions can be drawn:

- The porous UNC exhibited a much higher electrochemically active surface area and a faster electron transfer than the flat and the standard electrodes evaluated in this work. The three electrodes show quasi reversible behaviors with the $Fe(CN)_6^{3-}/Fe(CN)_6^{4-}$ redox pair.
- The three tested electrodes show a high reproducibility in terms of oxidant production. Results show that there is a very important influence of the diamond coating of the production of oxidants during the electrolysis of solutions containing phosphoric acid (acid pH) or phosphate salts (at alkaline pHs). Despite not exhibiting the largest electrochemical surface area, the flat UNC electrode shows the best performance for this process, except for the operation at low current densities and alkaline pHs in which the porous UNC outperforms it.
- Better efficiencies are obtained operating at mild current densities which was explained in terms of the great significance of direct processes in the production of oxidants by electrolysis of phosphoric acid or phosphate solutions.

- Alkaline pH allows to obtain higher concentrations of oxidants, and this is explained in terms of a promotion in the direct oxidation of phosphate and biphosphate anions to phosphate radicals and their combination. As well because of the much lower effect of the scavengers in that range of pH conditions. Performance of acidic electrolysis should be explained in terms of the role of hydroxyl radicals.

Acknowledgements

This work comprises the research project PDC2021-121105-I00 granted by MCIN/ AEI/10.13039/501100011033/ and "Unión Europea NextGenerationEU/PRTR". The authors also acknowledge the financial support provided by Brazilian funding agencies including the Brazilian National for Scientific and Technological Development (CNPq - grant #303943/2021-1) and São Paulo Research Foundation (FAPESP – grants #2021/07615-7, #2019/00592-1, #2017/10118-0).

Declaration of competing interest

The authors declare that they have no known competing financial interests or personal relationships that could influence the work reported in this paper.

Author statement

L.G Vernasqui: investigation; writing – original draft; methodology; and data curation.

N.G. Ferreira: conceptualization; funding acquisition; supervision; and writing - review and editing.

C. Saez: conceptualization; funding acquisition; supervision; and writing - review and editing.

M.A. Rodrigo: conceptualization; funding acquisition; supervision; and writing - review and editing.

References

[1] K. Groenen Serrano, A critical review on the electrochemical production and use of peroxo-compounds, Curr Opin Electrochem. 27 (2021) 100679. https://doi.org/10.1016/j.coelec.2020.100679.

[2] C.A. Martínez-Huitle, M. Panizza, Electrochemical oxidation of organic pollutants for wastewater treatment, Curr Opin Electrochem. 11 (2018) 62–71. https://doi.org/10.1016/j.coelec.2018.07.010.

[3] W.P. Griffith, R.D. Powell, A.C. Skapski, Alkali metal and ammonium peroxodiphosphates: Preparation, vibrational and 31P NMR spectra, and the X-ray crystal structure of ammonium peroxodiphosphate dihydrate (NH4)4[P2O8]·2H2O, Polyhedron. 7 (1988) 1305–1310. https://doi.org/10.1016/S0277-5387(00)81228-0.

[4] L. Fijołek, J. Świetlik, M. Frankowski, The Role of Sulphate and Phosphate Ions in the Recovery of Benzoic Acid Self-Enhanced Ozonation in Water Containing Bromides, Molecules. 26 (2021) 2701. https://doi.org/10.3390/molecules26092701.

[5] A. Sánchez, J. Llanos, C. Sáez, P. Cañizares, M.A. Rodrigo, On the applications of peroxodiphosphate produced by BDD-electrolyses, Chemical Engineering Journal. 233 (2013) 8–13. https://doi.org/10.1016/j.cej.2013.08.022.

[6] P. Cañizares, C. Sáez, A. Sánchez-Carretero, M.A. Rodrigo, Synthesis of novel oxidants by electrochemical technology, J Appl Electrochem. 39 (2009) 2143–2149. https://doi.org/10.1007/s10800-009-9792-7.

[7] C.J. Battaglia, J.O. Edwards, The Dissociation Constants and the Kinetics of Hydrolysis of Peroxymonophosphoric Acid, Inorg Chem. 4 (1965) 552–558. https://doi.org/10.1021/ic50026a024.

[8] G. Muthuraman, M. Thirumavalavan, M. Il Shik, In situ electrochemically generated peroxymonophosphoric acid as an oxidant for the effective removal of gaseous acetaldehyde, Chemical Engineering Journal. 325 (2017) 449–456. https://doi.org/10.1016/j.cej.2017.05.068.

[9] A. Kraft, M. Stadelmann, M. Blaschke, Anodic oxidation with doped diamond electrodes: a new advanced oxidation process, J Hazard Mater. 103 (2003) 247–261. https://doi.org/10.1016/j.jhazmat.2003.07.006.

[10] P. Cañizares, F. Larrondo, J. Lobato, M.A. Rodrigo, C. Sáez, Electrochemical Synthesis of Peroxodiphosphate Using Boron-Doped Diamond Anodes, J Electrochem Soc. 152 (2005) D191. https://doi.org/10.1149/1.2039936.

[11] E. Weiss, C. Sáez, K. Groenen-Serrano, P. Cañizares, A. Savall, M.A. Rodrigo, Electrochemical synthesis of peroxomonophosphate using boron-doped diamond anodes, J Appl Electrochem. 38 (2007) 93–100. https://doi.org/10.1007/s10800-007-9405-2.

[12] O. Kirk, Encyclopedia of chemical technology, 4th ed., Wiley-Interscience Publications, New York, 1996.

[13] D.M. de Araújo, C. Sáez, P. Cañizares, M.A. Rodrigo, C.A. Martínez-Huitle, Improving the catalytic effect of peroxodisulfate and peroxodiphosphate electrochemically generated at diamond electrode by activation with light irradiation, Chemosphere. 207 (2018) 774–780. https://doi.org/10.1016/j.chemosphere.2018.05.121.

[14] J. Wang, S. Wang, Activation of persulfate (PS) and peroxymonosulfate (PMS) and application for the degradation of emerging contaminants, Chemical Engineering Journal. 334 (2018) 1502–1517. https://doi.org/10.1016/j.cej.2017.11.059.

[15] J. Li, Y. Ren, L. Lai, B. Lai, Electrolysis assisted persulfate with annular iron sheet as anode for the enhanced degradation of 2, 4-dinitrophenol in aqueous solution, J Hazard Mater. 344 (2018) 778–787. https://doi.org/10.1016/j.jhazmat.2017.11.007.

[16] M. Nie, C. Yan, X. Xiong, X. Wen, X. Yang, Z. lv, W. Dong, Degradation of chloramphenicol using a combination system of simulated solar light, Fe2+ and persulfate, Chemical Engineering Journal. 348 (2018) 455–463. https://doi.org/10.1016/j.cej.2018.04.124.

[17] L. Bu, S. Zhou, Z. Shi, L. Deng, N. Gao, Removal of 2-MIB and geosmin by electrogenerated persulfate: Performance, mechanism and pathways, Chemosphere. 168 (2017) 1309–1316. https://doi.org/10.1016/j.chemosphere.2016.11.134.

[18] J. Cai, M. Zhou, W. Yang, Y. Pan, X. Lu, K.G. Serrano, Degradation and mechanism of 2,4-dichlorophenoxyacetic acid (2,4-D) by thermally activated persulfate oxidation, Chemosphere. 212 (2018) 784–793. https://doi.org/10.1016/j.chemosphere.2018.08.127.

[19] I.F. Mena, S. Cotillas, E. Díaz, C. Sáez, Á.F. Mohedano, M.A. Rodrigo, Influence of the supporting electrolyte on the removal of ionic liquids by electrolysis with diamond anodes, Catal Today. 313 (2018) 203–210. https://doi.org/10.1016/j.cattod.2017.10.025.

[20] J.M. Aquino, M.A. Rodrigo, R.C. Rocha-Filho, C. Sáez, P. Cañizares, Influence of the supporting electrolyte on the electrolyses of dyes with conductive-diamond anodes, Chemical Engineering Journal. 184 (2012) 221–227. https://doi.org/10.1016/j.cej.2012.01.044.

[21] C.R. Costa, F. Montilla, E. Morallón, P. Olivi, Electrochemical oxidation of acid black 210 dye on the boron-doped diamond electrode in the presence of phosphate ions: Effect of current density, pH, and chloride ions, Electrochim Acta. 54 (2009) 7048–7055. https://doi.org/10.1016/j.electacta.2009.07.027.

[22] P. Canizares, C. Sáez, F. Martínez, M.A. Rodrigo, The role of the characteristics of p-Si BDD anodes on the efficiency of wastewater electro-oxidation processes, Electrochemical and Solid-State Letters. 11 (2008). https://doi.org/10.1149/1.2916436.

[23] I. Moraleda, S. Cotillas, J. Llanos, C. Sáez, P. Cañizares, L. Pupunat, M.A. Rodrigo, Can the substrate of the diamond anodes influence on the performance of the electrosynthesis of oxidants?, Journal of Electroanalytical Chemistry. 850 (2019) 113416. https://doi.org/10.1016/j.jelechem.2019.113416.

[24] F.A. Souza, A.F. Azevedo, C. Giles, E. Saito, M.R. Baldan, N.G. Ferreira, The effect of boron doping level on the morphology and structure of ultra/nanocrystalline diamond films, Chemical Vapor Deposition. 18 (2012) 159–165. https://doi.org/10.1002/cvde.201106953.

[25] L.G. Vernasqui, B.A. Kawata, A.F. Sardinha, M.A. Rodrigo, N.G. Ferreira, Achievement and electrochemical responsiveness of advanced boron-doped ultrananocrystalline diamond on highly ordered titanium dioxide nanotubes, Diam Relat Mater. 121 (2022) 108793. https://doi.org/10.1016/j.diamond.2021.108793.

[26] R. Mei, Q. Wei, C. Zhu, W. Ye, B. Zhou, L. Ma, Z. Yu, K. Zhou, 3D macroporous boron-doped diamond electrode with interconnected liquid flow channels: A high-efficiency electrochemical degradation of RB-19 dye wastewater under low current, Appl Catal B. 245 (2019) 420–427. https://doi.org/10.1016/j.apcatb.2018.12.074.

[27] N. Elgrishi, K.J. Rountree, B.D. McCarthy, E.S. Rountree, T.T. Eisenhart, J.L. Dempsey, A Practical Beginner's Guide to Cyclic Voltammetry, J Chem Educ. 95 (2018) 197–206. https://doi.org/10.1021/acs.jchemed.7b00361.

[28] I.M. Kolthoff, E.M. Carr, Volumetric Determination of Persulfate in Presence of Organic Substances, Anal Chem. 25 (1953) 298–301. https://doi.org/10.1021/ac60074a024.

[29] P.W. May, M.N.R. Ashfold, Y.A. Mankelevich, Microcrystalline, nanocrystalline, and ultrananocrystalline diamond chemical vapor deposition: Experiment and modeling of the factors controlling growth rate, nucleation, and crystal size, J Appl Phys. 101 (2007). https://doi.org/10.1063/1.2696363.

[30] S. Bühlmann, E. Blank, R. Haubner, B. Lux, Characterization of ballas diamond depositions, Diam Relat Mater. 8 (1999) 194–201. https://doi.org/10.1016/S0925-9635(98)00258-1.

[31] P.W. May, Y.A. Mankelevich, From Ultrananocrystalline Diamond to Single Crystal Diamond Growth in Hot Filament and Microwave Plasma-Enhanced CVD Reactors: a Unified Model for Growth Rates and Grain Sizes, The Journal of Physical Chemistry C. 112 (2008) 12432–12441. https://doi.org/10.1021/jp803735a.

[32] M.H. Nazare, A.J. Neves, Properties, Growth and Applications of Diamond, EMIS datareviews, London, United Kingdom, 2011.

[33] T.-S. Yang, J.-Y. Lai, M.-S. Wong, C.-L. Cheng, Combined effects of argon addition and substrate bias on the formation of nanocrystalline diamond films by chemical vapor deposition, J Appl Phys. 92 (2002) 4912–4917. https://doi.org/10.1063/1.1512320.

[34] J.A. Carlisle, O. Auciello, Ultrananocrystalline Diamond Properties and Applications in Biomedical Devices, Electrochem Soc Interface. 12 (2003) 28–31. https://doi.org/10.1149/2.F08031IF.

[35] R.-X. He, D.-W. Zha, Cyclic voltammetry and voltabsorptometry studies of redox mechanism of lumazine, Journal of Electroanalytical Chemistry. 791 (2017) 103–108. https://doi.org/10.1016/j.jelechem.2017.03.026.

[36] F. Liu, Z. Deng, D. Miao, W. Chen, Y. Wang, K. Zhou, L. Ma, Q. Wei, A highly stable microporous boron-doped diamond electrode etched by oxygen plasma for enhanced

electrochemical ozone generation, J Environ Chem Eng. 9 (2021) 106369. https://doi.org/10.1016/j.jece.2021.106369.

[37] M. Rajab, C. Heim, T. Letzel, J.E. Drewes, B. Helmreich, Electrochemical disinfection using boron-doped diamond electrode – The synergetic effects of in situ ozone and free chlorine generation, Chemosphere. 121 (2015) 47–53. https://doi.org/10.1016/j.chemosphere.2014.10.075.

[38] G. Santana-Martínez, G. Roa-Morales, L. Gómez-Olivan, E. Peralta-Reyes, R. Romero, R. Natividad, Downflow bubble column electrochemical reactor (DBCER): In-situ production of H2O2 and O3 to conduct electroperoxone process, J Environ Chem Eng. 9 (2021) 105148. https://doi.org/10.1016/j.jece.2021.105148.

[39] T. Watanabe, Y. Honda, K. Kanda, Y. Einaga, Tailored design of boron-doped diamond electrodes for various electrochemical applications with boron-doping level and sp^2-bonded carbon impurities, Physica Status Solidi (a). 211 (2014) 2709–2717. https://doi.org/10.1002/pssa.201431455.

[40] P.J. Espinoza-Montero, P. Alulema-Pullupaxi, B.A. Frontana-Uribe, C.E. Barrera-Diaz, Electrochemical production of hydrogen peroxide on Boron-Doped diamond (BDD) electrode, Curr Opin Solid State Mater Sci. 26 (2022) 100988. https://doi.org/10.1016/j.cossms.2022.100988.

[41] P.J. Espinoza-Montero, P. Alulema-Pullupaxi, B.A. Frontana-Uribe, C.E. Barrera-Diaz, Electrochemical production of hydrogen peroxide on Boron-Doped diamond (BDD) electrode, Curr Opin Solid State Mater Sci. 26 (2022) 100988. https://doi.org/10.1016/j.cossms.2022.100988.

[42] Y. Jiang, P. Ni, C. Chen, Y. Lu, P. Yang, B. Kong, A. Fisher, X. Wang, Selective Electrochemical H_2O_2 Production through Two-Electron Oxygen Electrochemistry, Adv Energy Mater. 8 (2018) 1801909. https://doi.org/10.1002/aenm.201801909.

[43] S. Mavrikis, M. Göltz, S. Rosiwal, L. Wang, C. Ponce de León, Boron-Doped Diamond Electrocatalyst for Enhanced Anodic H_2O_2 Production, ACS Appl Energy Mater. 3 (2020) 3169–3173. https://doi.org/10.1021/acsaem.0c00093.

[44] M. Rodríguez-Peña, J.A. Barrios Pérez, J. Llanos, C. Saez, C.E. Barrera-Díaz, M.A. Rodrigo, Is ozone production able to explain the good performance of CabECO® technology in wastewater treatment?, Electrochim Acta. 396 (2021) 139262. https://doi.org/10.1016/j.electacta.2021.139262.

[45] M. Rodríguez-Peña, J.A. Barrios Pérez, J. Llanos, C. Saez, C.E. Barrera-Díaz, M.A. Rodrigo, Electrochemical generation of ozone using a PEM electrolyzer at acidic pHs, Sep Purif Technol. 267 (2021) 118672. https://doi.org/10.1016/j.seppur.2021.118672.

[46] M. Rodríguez-Peña, J.A.B. Pérez, J. Llanos, C. Saez, C.E. Barrera-Díaz, M.A. Rodrigo, Understanding ozone generation in electrochemical cells at mild pHs, Electrochim Acta. 376 (2021) 138033. https://doi.org/10.1016/j.electacta.2021.138033.

[47] M. Rodríguez-Peña, J.A. Barrios Pérez, J. Llanos, C. Sáez, M.A. Rodrigo, C.E. Barrera-Díaz, New insights about the electrochemical production of ozone, Curr Opin Electrochem. 27 (2021) 100697. https://doi.org/10.1016/j.coelec.2021.100697.

[48] P. Cañizares, C. Sáez, J. Lobato, R. Paz, M.A. Rodrigo, Effect of the Operating Conditions on the Oxidation Mechanisms in Conductive-Diamond Electrolyses, J Electrochem Soc. 154 (2007) E37. https://doi.org/10.1149/1.2424409.

[49] S. Anantharaj, S. Noda, How properly are we interpreting the Tafel lines in energy conversion electrocatalysis?, Mater Today Energy. 29 (2022) 101123. https://doi.org/10.1016/j.mtener.2022.101123.